Ibn Al-Haitham Journal for Pure and Applied Sciences
Journal homepage: jih.uobaghdad.edu.iq
PISSN: 1609-4042, EISSN: 2521-3407
IHJPAS. 2026; 39(2)

Synthesis and Spectral Investigation of Mixed Schiff Base and L-Leucine Complexes and their Biological Activity

Maysam Basem Abdulsalam[1], Taghreed Hashim AL-Noor*[2],and Aly Abdou[3]
[1,2]Department of Chemistry, College of Education for Pure Science (Ibn Al-Haitham), University of Baghdad, Baghdad, Iraq
[3]Department of Chemistry, Faculty of Science, Sohag University, Sohag, 82524 Egypt
*Corresponding Author

Received: 1/December/2025
Accepted: 8/February/2026
Published: 20/April/2026
doi.org/10.30526/39.2.4340

Abstract

In this study, transition complexes of Fe(III), Zn(II), La(III), Ce(III), and Pr(III) with a Schiff base ligand (L), which is derived from 3-hydroxybenzaldehyde and sulfamethoxazole, as the primary ligand, and L-Leucinate as a secondary ligand. The bonding mode of the Schiff base has been confirmed through a range of techniques, including infrared, UV-visible (UV-Vis), carbon and proton nuclear magnetic resonance spectroscopy, mass spectrometry, and elemental analysis. All complexes were characterized by elemental analysis, conductivity measurements, and spectroscopic techniques, including UV-Vis and Fourier transform infrared spectroscopy. A thorough discussion is provided on the structural and bonding features of the mixed ligand complexes formed from the Schiff base (L) and L-Leucine with ions [Fe (III), Zn(II), La(III), Ce(III), and Pr(III)], based on results from various research studies. Additionally, the antimicrobial activity of these complexes was evaluated against two Gram-positive and two Gram-negative bacterial strains. Furthermore, antifungal activity against *Candida* was evaluated, with tetracycline as the reference.

Keywords: Biological activity, L-Leucine, Schiff base, Sulfonamides, Transition metal.

1. Introduction

Sulfonamides are bacteriostatic antibiotics that contain the functional group ($R\text{-}SO_2\text{-}N<R_1R_2$, R_1/R_2= H, alkyl, aryl, and hetero aryl groups) that compounds to inhibit the growth of microorganisms1. They are widely used in the treatment of urinary, respiratory, and skin infections; gastrointestinal, antifungal, antioxidant, anti-inflammatory, diuretic, antiviral, carbonic anhydrase, anticancer, antidiabetic, antitubercular, and antimalarial[1,2]. Sulfamethoxazole (SMX) is a broad-spectrum antibiotic employed in human and veterinary medicine, belonging to the sulfonamide class of pharmaceuticals (sulfa drugs)[3]. SMX is known as 4-amino-N-(5-methyl-1,2-oxazol-3-yl)benzenesulfonamide ($C_{10}H_{11}N_3O_3S$), a white, odorless, and tasteless compound[4]. It is commonly used to treat bacterial infections, including bronchitis; upper and lower respiratory tract infections; prostatitis; skin and subcutaneous infections; kidney and urinary tract infections; and genital infections[5]. Schiff bases are typically synthesized by reacting SMX with a specific aldehyde or ketone. Schiff bases are integral to coordination chemistry, serving as chelating agents in the form of Schiff base-metal complexes with extensive applications in clinical, analytical, and biological fields[6]. A Schiff base is composed of a (>C=N-R) structure. It is efficiently synthesized through a condensation reaction between a primary amine and an aldehyde or ketone[7]. The condensation of aromatic aldehydes (-CHO) and ketones (-CO-) with sulfonamides, as a source of arylamines, has led to the synthesis of Schiff bases, which have been shown to possess a broad spectrum of biological activities, including

antimicrobial, anti-inflammatory, antifungal, and antipyretic effects. The bactericidal activity of sulfonamides results from their inhibition of the competitive binding of *p*-aminobenzoic acid (PABA) within the folic acid metabolic pathway[8]. Transition metals are characterized by incompletely filled d- or f-electron shells in their neutral or cationic forms, and they readily receive electrons from ligands via their partially filled valence shell orbitals, thereby facilitating the formation of coordination complexes. Schiff base (imine); readily forms stable complexes with most transition metal ions and plays a significant role in both inorganic and bioinorganic chemistry[9]. Schiff bases tend to form coordination complexes with various transition metals, which form adducts between the azomethine nitrogen and the metal ion. There is global interest in the use of transition-metal complexes with Schiff bases in medicine[10]. This study aims to produce new Schiff base complexes by reacting the Schiff base ligand with L-Leucine and transition metals. This study employed thermal analysis, spectroscopy, and elemental analysis to elucidate the structures of novel substances. Additionally, the compounds produced were tested for antibacterial activity.

2. Materials and Methods

2.1. Materials and physic-chemical analysis

This study used compounds directly from Sigma or BDH without purification. The substances that were determined to be of Analar grade (BDH) included ethanol, dimethyl sulfoxide (DMSO), 3-hydroxybenzaldehyde (3-HBA), and SMX. The Fourier transform infrared (FTIR) spectra in the 400-4000 cm^{-1} area were recorded using the A224160-Shimadzu spectrophotometer at the Department of Chemistry, College of Education for Pure Science (Ibn Al-Haitham), University of Baghdad. Mass spectral data were acquired via an MS Model 5973 spectrometer and subsequently analyzed using elemental microanalysis. C.H.N.-2400 Elemental Analyzer at the Islamic Republic of Iran, University of Tehran. The INOVA-500 MHz spectrometer was employed to acquire the carbon and proton nuclear magnetic resonance (^{13}C, ^{1}H-NMR) spectra of (L) in deuterated dimethyl sulfoxide, with chemical shifts reported in parts per million (ppm) at the Islamic Republic of Iran, University of Tehran. A spectrophotometer (A.A-160) is employed to measure metal content at the Ibn Sina company in Baghdad, Iraq. Balance Gouy reported Johnson's measurements of magnetic moments in complexes at the College of Sciences, Al-Mustansiriyah University. The Ino. Lab. 720 digital conductivity meter was used to obtain a value of Λm 10^{-3} mol/L in ethanol at the Department of Chemistry, College of Education for Pure Science (Ibn Al-Haitham), University of Baghdad. The molecular structures of the compounds have been illustrated using the Chem-Sketch (2019) software.

2.2. Synthesis of Schiff base (L)

The Schiff base ligand (L) was synthesized through a condensation reaction involving the dissolution of 3-hydroxybenzaldehyde ($C_7H_6O_2$, molecular weight= 122 g/mol) and an equimolar amount of SMX ($C_{10}H_{11}N_3O_3S$, molecular weight= 253.3 g/mol) in 20 mL of ethanolic solution, with the addition of 4 to 5 drops of glacial acetic acid (CH_3COOH). The resulting mixture was heated and magnetically stirred for 6 hours at 80°C. The reaction was monitored using thin-layer chromatography (TLC). Evaporation at ambient temperature was used to gradually reduce the mixture volume after a full day of standing. The light-brown precipitate was repeatedly washed with absolute ethanol and subsequently recrystallized from ethanol to yield a purified sample. Yield: 80.52%, light brown, sample $C_{17}H_{15}N_3O_4S$, molecular weight= 357.38 g/mol, C.H.N analysis: % Calculated ,(% C: 57.13), (%H: 4.23), (%N: 11.76), (%S: 8.97). % Found: (%C: 56.92), (%H: 4.49), (%N: 11.35), (%S: 9.71). **Figure 1** illustrates the ligand structure.

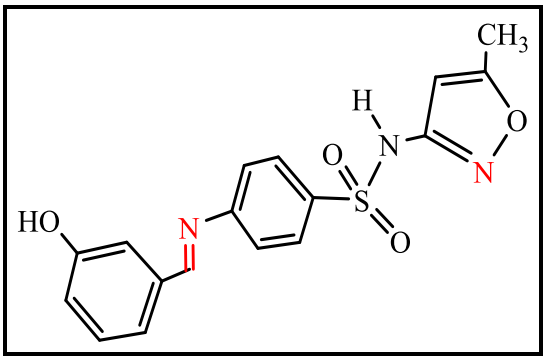

Figure 1. Structure of ligand (L)

2.3. General procedure for the synthesis of the mixed ligands chelates from (L) and L- leucine (L-Leu) with some metals ions

The first step was to dissolve L-leucine (0.131 g, 1 mmol) in a 10 mL mixture of H_2O and ethanol (1:1) containing KOH (0.056 g, 1 mmol). It was stirred at room temperature to prepare potassium L-leucinate[11]. Then by combining equal amounts of ethanolic solutions of the ligand (L), potassium leucinate (K-Leu), and metal chloride salts ($FeCl_3$), ($ZnCl_2$), ($LaCl_2•7H_2O$), ($CeCl_2•7H_2O$), and ($PrCl_3$) in a 1:1:1 molar ratio within a 15 mL ethanol solvent, the chelates were isolated with a moderate yield ranging from 65% to 79%. The entire mixture was refluxed for six hours. The reaction was monitored by thin-layer chromatography (TLC), and the product was recrystallized multiple times from an alcoholic solution, then evaporated and stored in a desiccator. All complexes were synthesized using identical methods, as illustrated in **Scheme 1**.

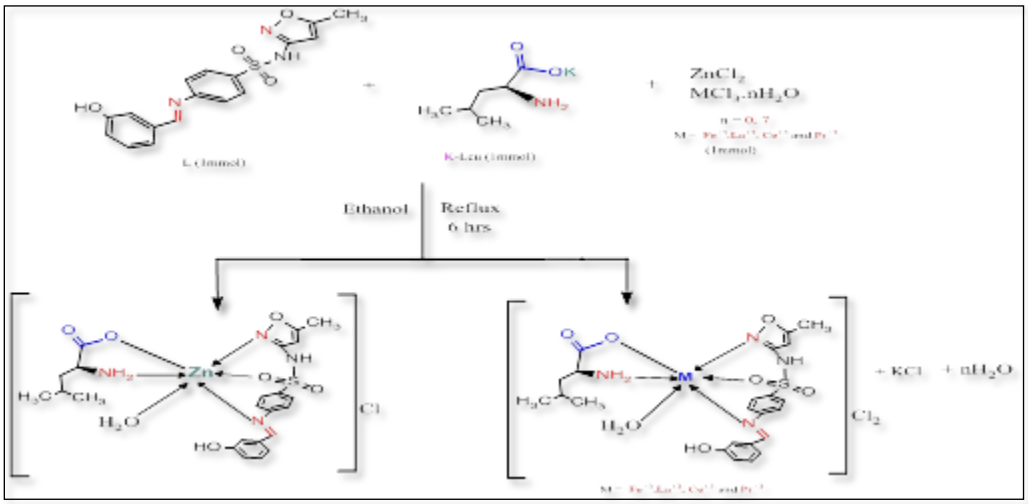

Scheme 1. Synthesis route of complexes

3. Results

3.1. Characterization of the Schiff base L

Elemental microanalysis, melting point determination, and spectroscopic techniques were employed to characterize the ligand (L). These techniques included FTIR spectroscopy, mass spectrometry, ^1H and ^{13}C-NMR spectroscopy, and UV-Vis spectroscopy. The ligand exhibits differing solubility in common organic solvents, being insoluble in water and benzene. It is soluble in methanol, ethanol, dimethylformamide, and dimethyl sulfoxide.

3.2. Data spectroscopic analysis

The NMR spectral data acquired using deuterated DMSO-d^6 as the solvent indicate that all proton and carbon atoms in the molecular structure are located in their predicted regions.

3.2.1. Data analysis of the ^{13}C-NMR spectrum of the L

The ^{13}C-NMR (ppm, d^6-DMSO, 400 MHz) spectrum of L shows a δ= 12 ppm signal corresponding to the methyl group attached to C_{25}. There is a δ = 95 ppm signal attributable to carbon in the isoxazole ring. δ= 113–138 ppm, aromatic carbon signals (C_{Ar}). The chemical shifts at δ= 153 ppm and δ= 158 ppm are assigned to C_{20} (C=N-O) of the isoxazole ring and C_{11} (C-OH) of the aromatic ring, respectively. The chemical shift at δ= 163 ppm is assigned to C_4 of the aromatic ring adjacent to the Schiff base. The aforementioned peak at δ= 170 ppm corresponds to C_{22} of the (C–O) group of the isoxazole ring, as illustrated in **Figure 2**.

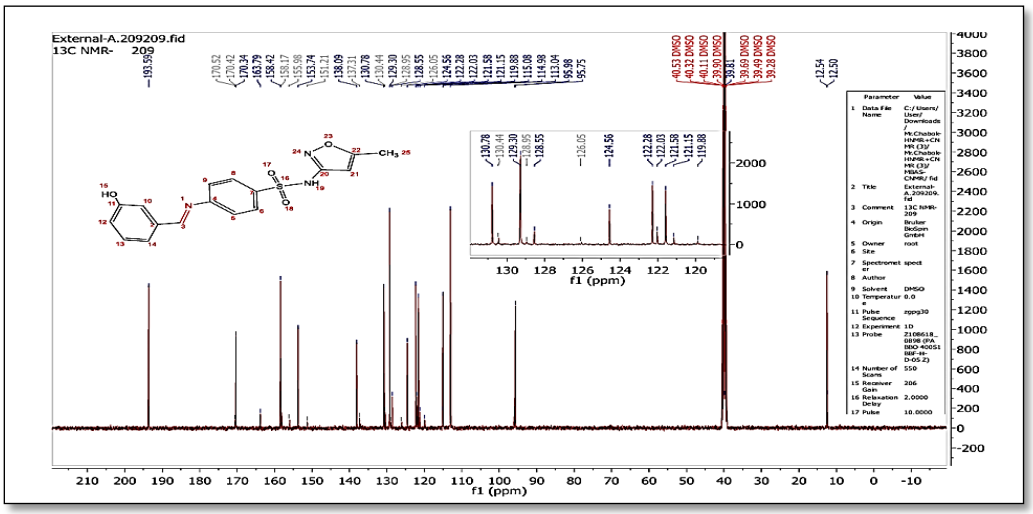

Figure 2. The ^{13}C-NMR spectrum of the L

3.2.2. Data analysis of the ^{1}H-NMR spectrum of the L

The ^{1}H-NMR spectrum (ppm, d^6-DMSO, 400 MHz) of ligand (L) is shown in **Figure 3**.

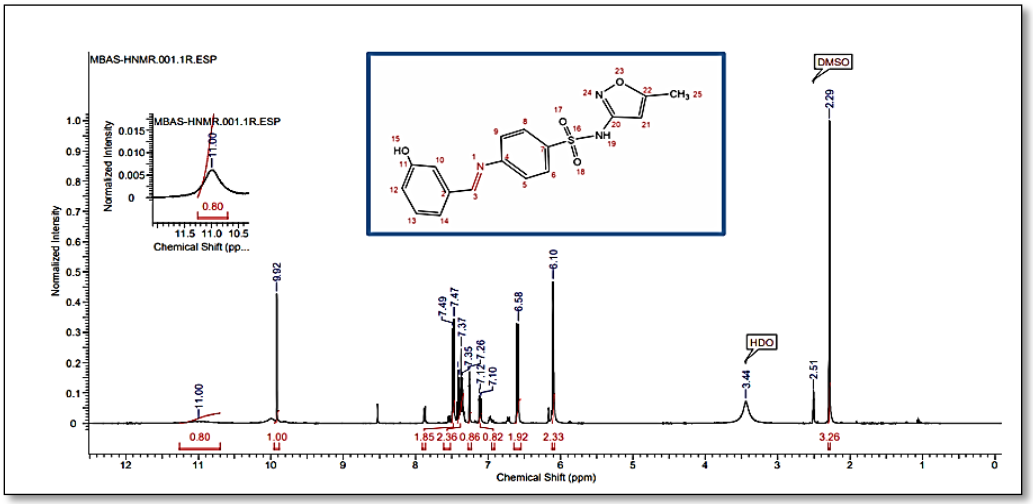

Figure 3. The ^{1}H-NMR spectrum of the L

3.3. Data analysis of the mass spectrum of L

The molecular weight and fragmentation pattern of L, along with its mass spectrum, were ascertained through mass spectrometry, as shown in **Figure 4**. The calculated m/z spectrum is 357.38, while the observed value is 357.35, which corresponds to the mass of the ligand.

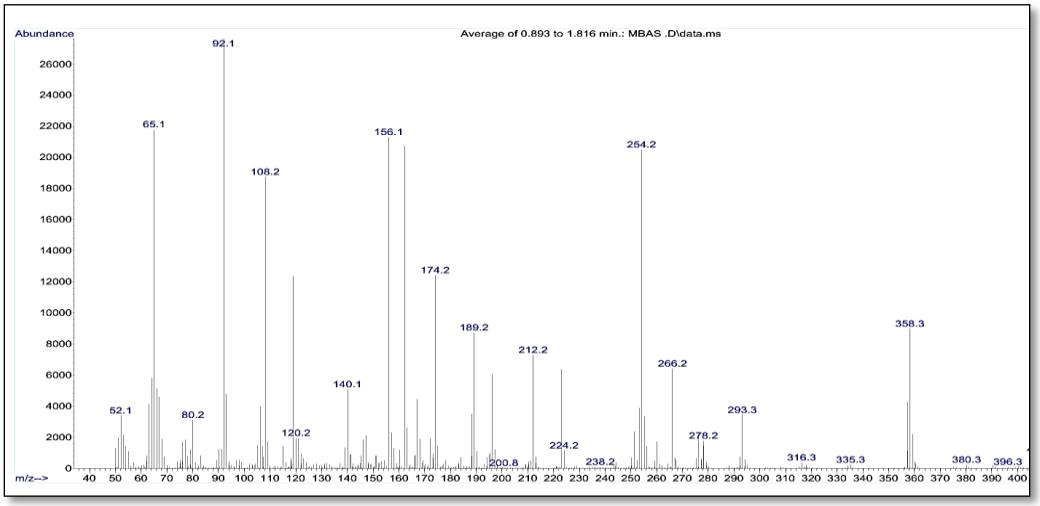

Figure 4. ESI-MS for ligand L

3.4. Data analysis of the thermogravimetric (TGA)

The TG-DTA analysis of the L sample was conducted using helium as an inert gas at a flow rate of 20 mL/min over a temperature range of 20–700°C. The thermal stability, decomposition behavior, and water (H_2O) content of the compounds must be determined by thermal analysis conducted at a controlled heating rate. The TGA contours are depicted in **Figure 5**, and the thermal degradation profile displays four decomposition peaks, as detailed in **Table 1**.

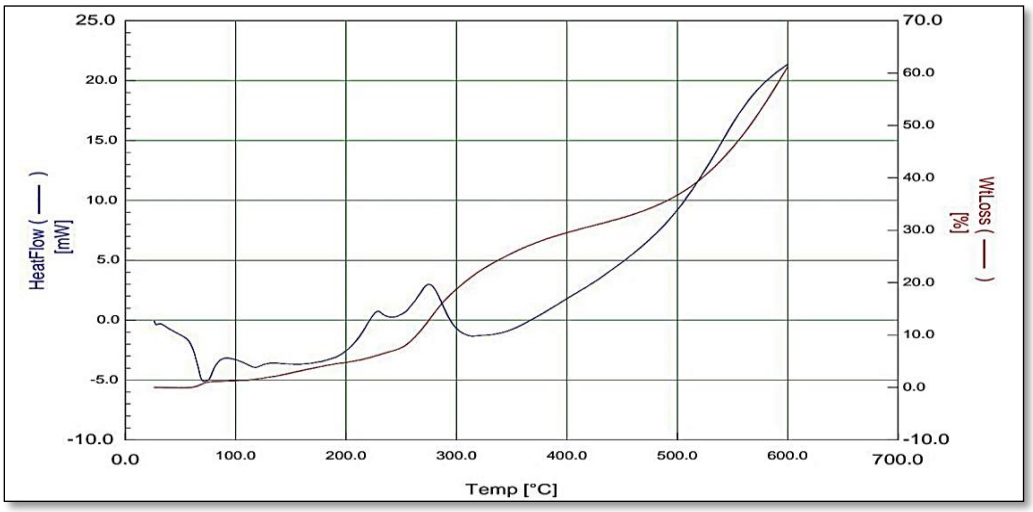

Figure 5. TGA–DTGA curves of the ligand L

Table 1. Steps thermal analysis of the ligand L

Steps	Decomposition Temperature ℃	Molar mass loss	Assignments
1	175	26.7	**-C-CH_3**
2	390	105.4	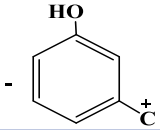
3	495	123	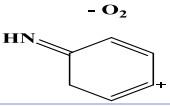

3.5. Data analysis of FTIR spectra of the compounds

Data analysis of FT-IR spectra for the complexes are illustrated in **Figures 6-11** and **Table 2**.

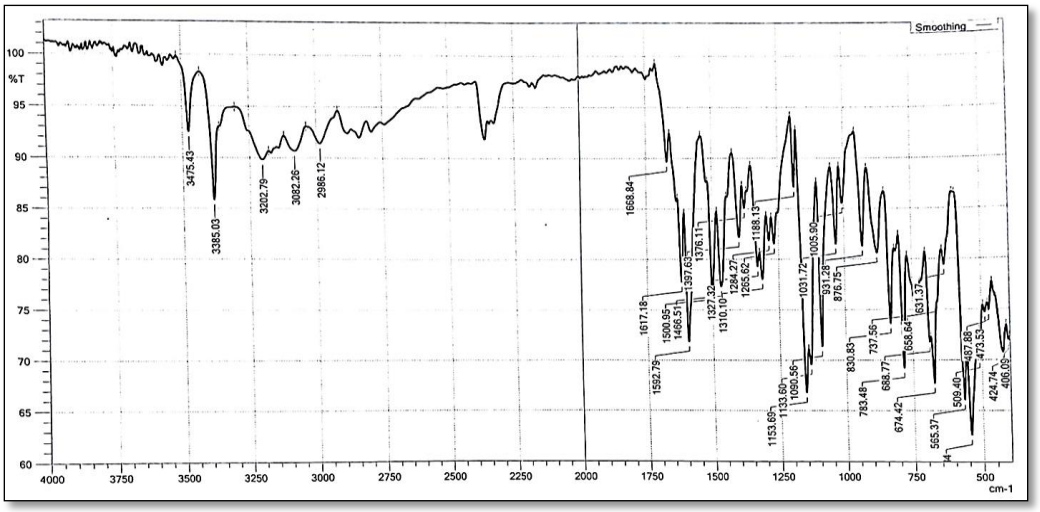

Figure 6. FTIR spectrum of ligand L

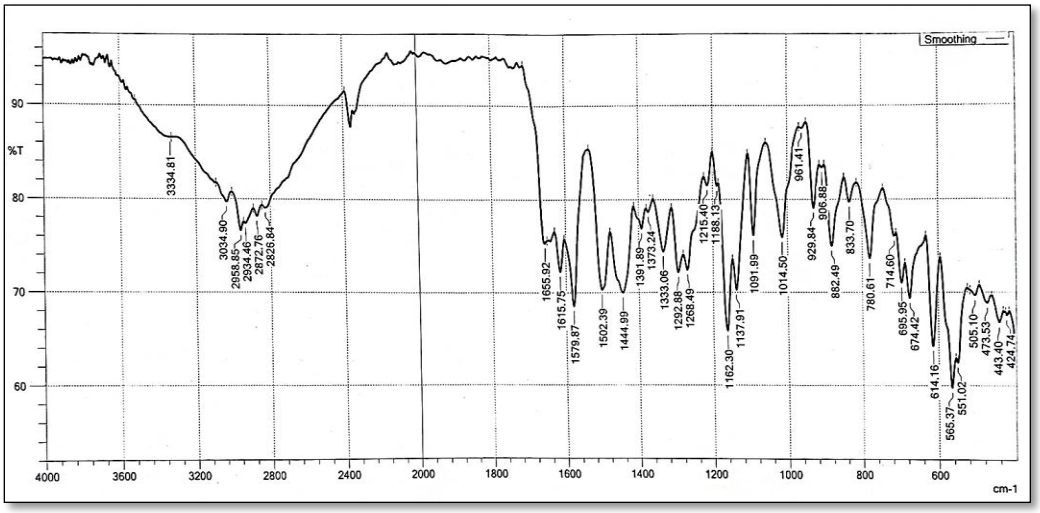

Figure 7. FTIR spectrum of $[Fe(L)(L\text{-}Leu)H_2O]Cl_2$

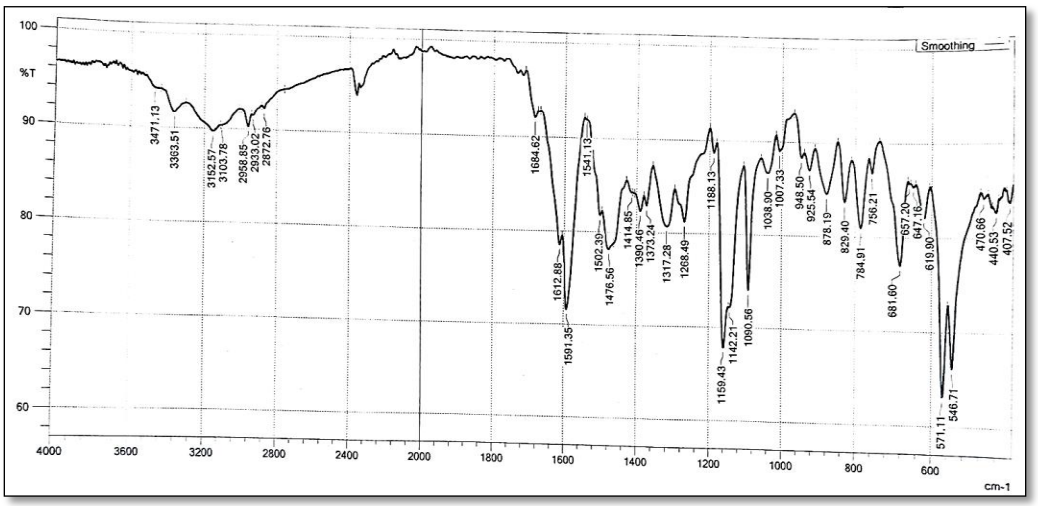

Figure 8. FTIR spectrum of $[Zn(L)(L\text{-}Leu)H_2O]Cl$

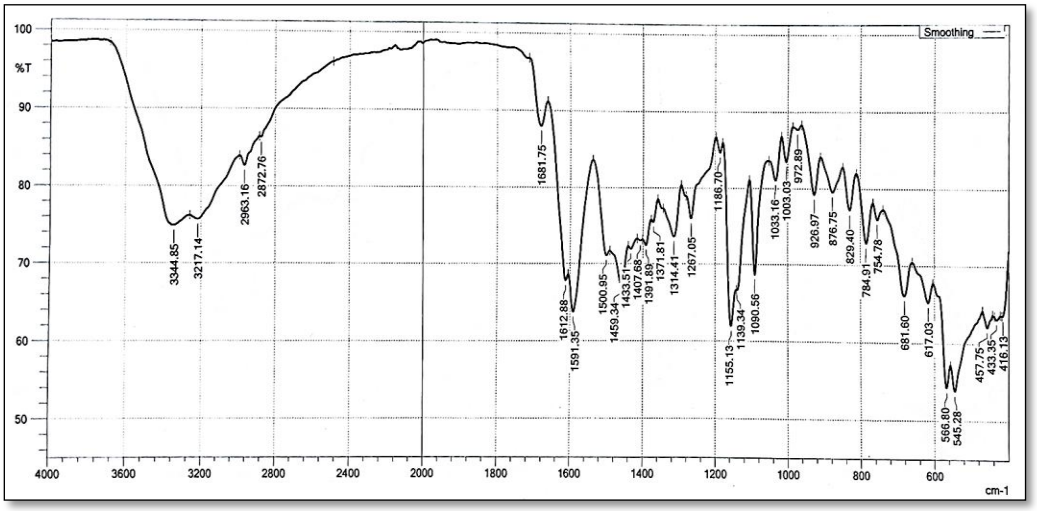

Figure 9. FTIR spectrum of $[La(L)(L\text{-}Leu)H_2O]Cl_2$

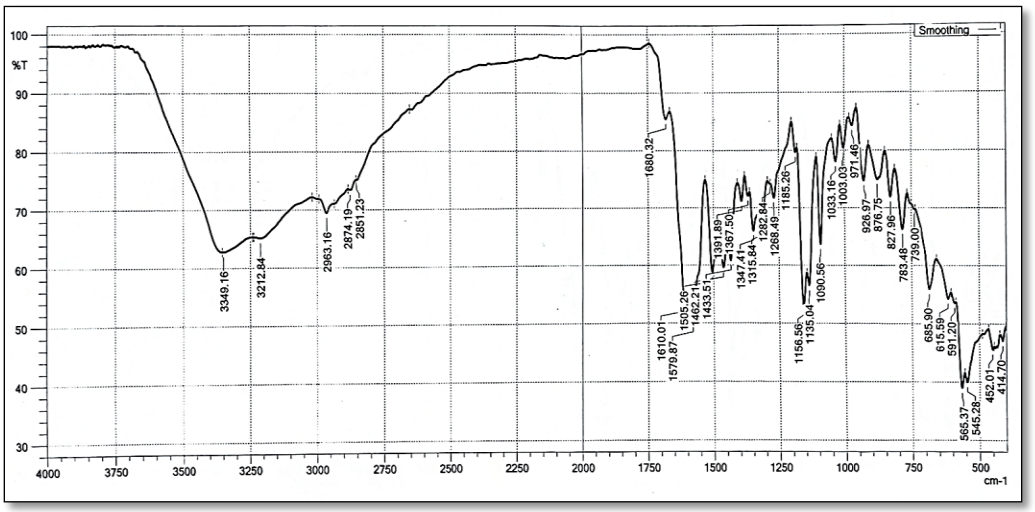

Figure 10. FTIR spectrum of $[Ce(L)(L\text{-}Leu)H_2O]Cl_2$

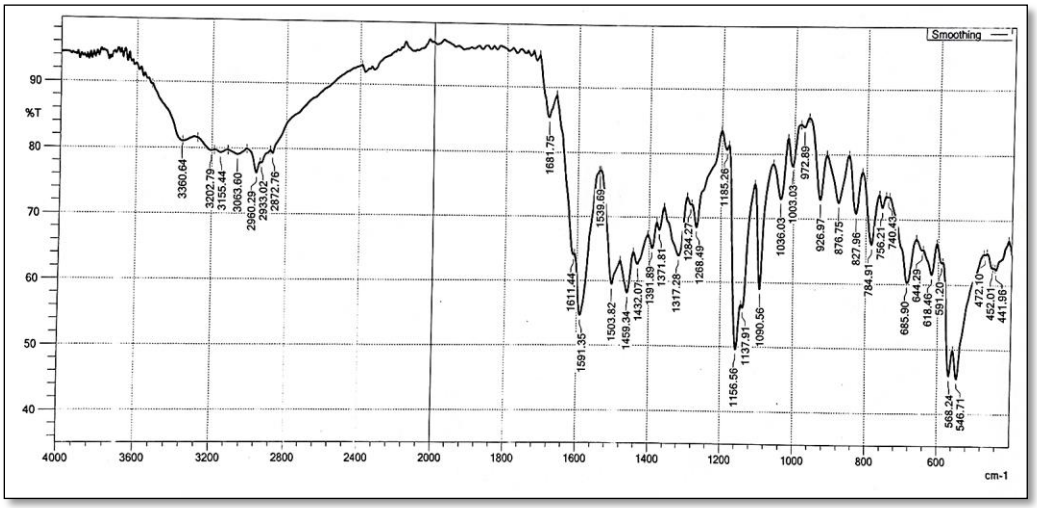

Figure 11. FTIR spectrum of $[Pr(L)(L\text{-}Leu)H_2O]Cl_2$

Table 2. Infrared spectral data (wave number ύ) cm^{-1} for complexes

Complexes / Stretching bands	Fe (III)	Zn(II)	La(III)	Pr(III)	Ce(III)
ν (N-H) ν (O-H) / H_2O	3334 Over lape	3471, 3363, 3152	3344, 3217	3360, 3202, 3155	3349, 3212
ν $(C=O)_{carb.}$	1655	1684	1681	1681	1680
ν $(C-H)_{aliph.}$	2958, 2937	2958, 2933	2963, 2872	2960, 2933	2963, 2874
ν $(C-H)_{aroma.}$	3034	3103	---	3063	---
N (C=N) isoxazole ring, ν $(C=N)_{Schiff}$	1615	1612	1612	1611	1610
ν (C=C)	1502	1502	1500	1503	1505
ν $(S=O)_{asym.}$ ν $(S=O)_{sym.}$	1391, 1137	1390, 1142	1391, 1139	1391, 1137	1397, 1135
$\nu_{asym.}$ $\nu_{sym.}$ (COO-)	1579, 1373	1591, 1373	1591, 1371	1591, 1371	1579, 1367
ν (C-O)	1268	1268	1267	1268	1268
ν (C-S)	833	829	829	827	827
ν(S-N)	929	925	926	926	926
ν (N-O)	1292	1317	1314	1317	1315
ν (M-N)	424, 443	407, 440	416, 433	441, 452	414, 452
ν (M-O)	551, 565	546, 571	545, 566	546, 568	545, 565

aliph. = aliphatic, aroma. = aromatic, carbo. = carboxylic, ν = stretching, asym. = asymmetry, sym. = symmetry.

3.6. UV-Vis spectral data of the compounds

The UV-Vis spectral data of the complexes are presented in **Figure 12**.

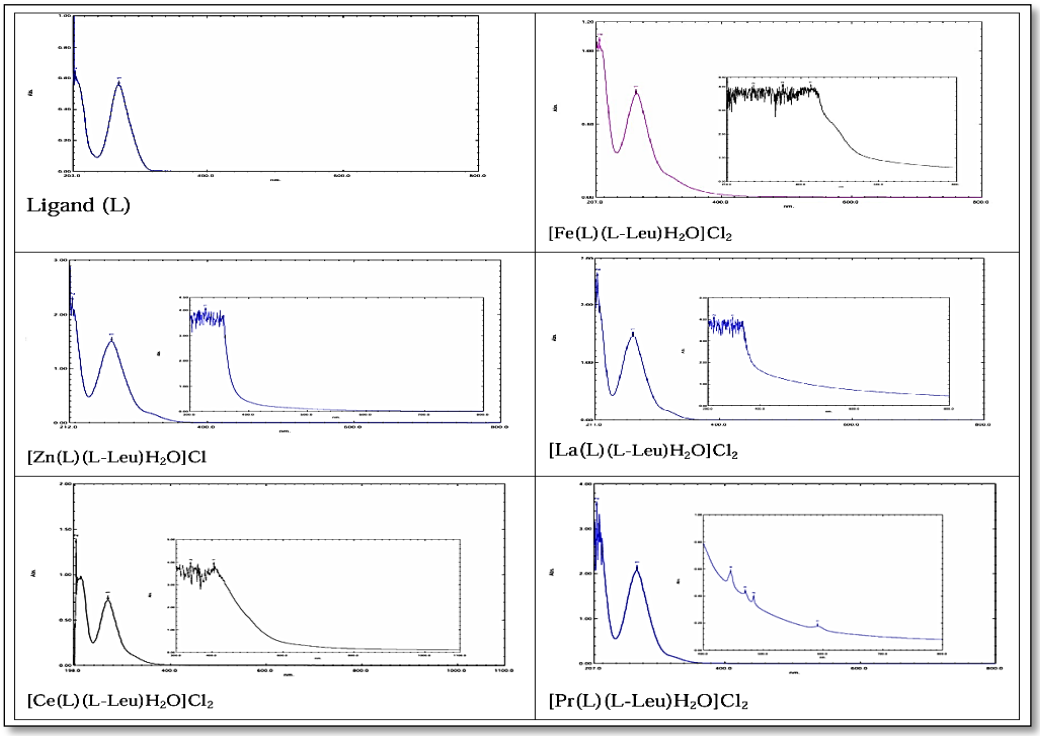

Figure 12. UV/Vis spectra of ligand and their complexes

3.7. Data of the antimicrobial screening

The examination of ligands and their metal complexes against a single fungal species (*Candida albicans*) and four bacterial species was performed using the agar-well diffusion method. The bacterial species included *Escherichia coli* and *Proteus mirabilis* (both Gram-negative), as well as *Bacillus subtilis* and *Staphylococcus aureus* (both Gram-positive). In this technique, a sterile metallic auger was used to form wells in the medium, maintaining a minimum spacing of 6 mm

between wells. The test samples were dissolved in DMSO to a final concentration of 1 mg/mL and injected into the designated wells at the specified concentration (10^{-3} M). The dishes containing bacterial and fungal species were incubated at 28°C and 37°C, respectively, for 24 to 48 hours. The activity was evaluated by determining the diameters of the inhibition zones (mm). The information documented and depicted in **Figure 13** is utilized to derive the following conclusions.

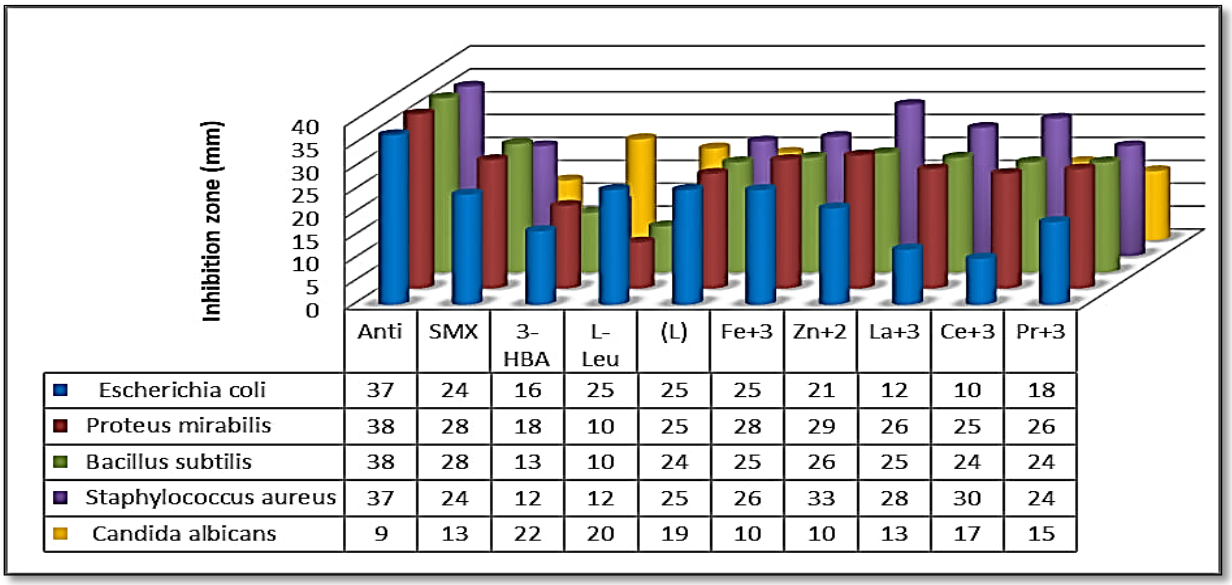

	Anti	SMX	3-HBA	L-Leu	(L)	Fe+3	Zn+2	La+3	Ce+3	Pr+3
Escherichia coli	37	24	16	25	25	25	21	12	10	18
Proteus mirabilis	38	28	18	10	25	28	29	26	25	26
Bacillus subtilis	38	28	13	10	24	25	26	25	24	24
Staphylococcus aureus	37	24	12	12	25	26	33	28	30	24
Candida albicans	9	13	22	20	19	10	10	13	17	15

Figure 13. Evolution of ligands and their complexes against growth (*Escherichia coli, Proteus mirabilis, Bacillus subtilis, Staphylococcus aureus and Candida albicans)*

4. Discussion

4.1. FTIR spectra of complexes

The FTIR spectra of all complexes are depicted in **Table 2**. There are no notable differences in the vibrational frequencies of the complexes and their FTIR spectra are comparable. In this study, a shift of the predominant bands towards lower or higher frequencies was generally observed when comparing the FTIR spectra of the complexes with those of free L-Leu and (L). The main reason is probably the coordination of two ligands.

The chemical shift in DMSO solvent is observed at δ= 39 ppm[12,13], as shown in **Figure 2**. In addition, the carbon atom at δ= 193 ppm is assigned to C_3 in the (-HC=N-) Schiff base group[14]. **Figure 3** displays a peak observed at 2.29 ppm (singlet, 3H, CH_3), a multiplet between 6.10 and 7.49 ppm (integrating for 9H, C_{Ar}), a singlet at 7.35 ppm (1H, NH), a peak at 9.92 ppm (singlet, 1H, C=N), and additionally a signal at 11 ppm (singlet, 1H, OH, phenol)[15].

The formation of M-ν(C=N) Schiff base, ν(S=O), and ν(C=N) isoxazole coordination bonds is responsible for the blue and red shifts of the observed bands. Additionally, two distinct absorption bands were observed in the spectra of the complexes at (1579–1591) cm^{-1} and (1367–1373) cm^{-1}. These bands indicated the difference between ν(COO─)asym. and ν (COO-) sym. vibrational modes of the (COOH) groups. The distinction Δν= [ν (COO─)asym. ─ ν(COO─)sym.] < 200 cm^{-1} falls within the range of (206-220) cm^{-1}. This results in the carboxyl group coordinating monodentately to the metal ions. L-Leucine acts as a bidentate ligand, coordinating with the active donor atoms via the carboxyl oxygen (COO−) and the nitrogen atom of the amino group (←: NH_2)[16,17].

In FTIR complexes, the rise of new bands within the range of 545–571 cm^{-1} was attributed to ν (M–O) vibrations for the Fe(III), Zn(II), La(III), Ce(III), and Pr(III) complexes, indicating that the oxygen atoms of the ligands are involved in coordination with the metal ions. Furthermore, ν (M–N) was attributed to the emergence of new bands at (407– 452) cm^{-1} in the spectra of Fe(III),

Zn(II), La(III), Ce(III), and Pr(III) complexes[18-20]. The FTIR spectra for Fe(III), Zn(II), La(III), Ce(III), and Pr(III) complexes are shown in **Figures 7-11**.

4.2. UV-Vis spectral of the ligands L, (L-Leucine) and the mixed ligand complexes

For (L-Leu), one high intensity sharp peak at 270 nm (37037 cm^{-1}) was ascribed to ($\pi - \pi^*$) electronic transitions within the organic ligand.

For ligand L in ethanol solvent, the absorption spectrum exhibits a significant, sharply defined peak at 277 nm (35335 cm^{-1}), which corresponds to ($n–\pi^*$) electronic transitions within the organic ligand associated with aromatic double bond character[21].

For the mixed-ligand complexes, the observed ligand-field ($\pi\rightarrow\pi^*$) and ($n\bullet\pi^*$) transitions corresponded to regions in the electronic spectra of the complexes, with wavelengths spanning 268-387 nm. The mixed-ligand complexes are suggested to display absorption bands with wavelengths spanning 324-390 nm, which are ascribed to charge-transfer transitions[22].

The magnetic moment of the Fe(III) d^5 (Term 6S) is complex 4.88 B.M., which is close to that expected for octahedral Fe(III) complexes, and these values of magnetic moments are due to orbital contribution[23].

The UV/Vis spectrum for the [Fe(L)(L-Leu) H_2O] Cl_2 complex exhibits four transitions. The first and scorned peaks at (268) nm (37313) cm^{-1} (ε_{max}= 710 $molar^{-1}.cm^{-1}$) and (278) nm (35971) cm^{-1} (ε_{max}= 3960 $molar^{-1}.cm^{-1}$) are referring to the ligand field, the peak at (353) nm (28329) cm^{-1} (ε_{max}= 4000 $molar^{-1}.cm^{-1}$) to the intra-ligand charge transfer (INCT)), and show one band (d-d) transition at (425) nm (23529) cm^{-1} (ε_{max}= 400 $molar^{-1}.cm^{-1}$) which is ascribed to the ($^6A_1g^{(S)} \rightarrow {}^4A_1g^{(G)}$) transition. These results reveal the octahedral geometry for this complex[24].

The (U.V-Vis) spectrum for [Zn(L)(L-Leu) H_2O] Cl (d^{10}) complex revealed no peaks in the visible range. The bands that appeared in the spectrum of the Zn (II) complex at (269 nm) (37175 cm^{-1}) (ε_{max}=1500 $molar^{-1}.cm^{-1}$) and at (326 nm) (30675 cm^{-1}) (ε_{max}= 4000 $molar^{-1}.cm^{-1}$), could be attributed to the charge transfer transitions induced by the conjugated π system[25].

The electronic absorption spectrum of [La(L)(L-Leu) H_2O] Cl_2 complex shows three peaks at (268 nm) 37313cm^{-1} and (302 nm) 33113 cm^{-1}, which may be assigned to transitions to intra-ligand (L.F) transitions from π-π^* and $n\rightarrow\pi^*$ in the -C= O and C=N groups. The peak at (341 nm) 29329 cm^{-1} could be attributed to the charge transfer transitions induced by the conjugated π system [26].

The electronic absorption spectrum of [Ce(L)(L-Leu)H_2O]Cl_2 complex showed three peaks at (269 nm) 37175cm^{-1}, (340nm) 29412 cm^{-1}, which may be appointed to transitions to intra-ligand (L.F), and (405 nm) 24691cm^{-1}, which may be appointed to transitions to (CT) transitions from π-π^* and $n\rightarrow\pi^*$ in the -C= O and C=N groups[27].

The electronic absorption spectrum of [Pr(L)(L-Leu) H_2O] Cl_2 complex showed three peaks at (270 nm) 37037 cm^{-1}, and (445 nm) 22472 cm^{-1}, which may be attributed to transitions to intra ligand transitions from π-π^* and $n\rightarrow\pi^*$ in the -C= O and C=N groups. Additionally, peaks at (470 nm) 21277cm^{-1}, (484 nm) 20661 cm^{-1} and (591 nm) 16920 cm^{-1} are assigned to (f→f) transitions between the metal ion and the ligand[28]. **Figure 12** shows the UV/Vis spectrum for the ligand (L) and all complexes.

4.3. The antimicrobial screening

For ligand (L), (L-Leu) and [Fe(L)(L-Leu) H_2O] Cl_2 displayed similar activity in inhibiting *Escherichia coli* to the rest of the same mixed ligand complexes. [Zn(L)(L-Leu) H_2O] Cl_2 complex displayed a higher activity in inhibiting *Proteus mirabilis*, *Bacillus subtilis*, and *Staphylococcus aureus* than the rest of the same mixed ligand complexes and the ligands. [Ce(L)(L-Leu) H_2O] Cl complex showed a higher activity in inhibiting *Candida albicans* than the rest of the same mixed ligand complexes. Tetracycline was used as a standard antibiotic, and DMSO served as a negative control[29].

5. Conclusions

In this investigation, the Schiff base ligand (L) and its corresponding metal complexes were successfully synthesized and fully characterized. The ligand was investigated using proton and carbon nuclear magnetic resonance spectroscopy, infrared spectroscopy, ultraviolet–visible spectroscopy, and thermogravimetric analysis, which collectively confirmed its molecular structure, functional groups, electronic transitions, and thermal stability. In contrast, the synthesized metal complexes were characterized by infrared and ultraviolet–visible spectroscopy, and their biological activities were evaluated to assess their potential biological efficacy.

Acknowledgment

The authors thank their colleagues at the College of Education for Pure Sciences (Ibn Al-Haitham) for their cooperation in completing this work, and they appreciate everyone who participated in the study.

Conflict of Interest

The authors declare that they have no conflicts of interest.

Funding

None.

References

1. Mubassir M, Ahamd N, Baby N, Kumar A. Comprehensive review of Schiff base sulphonamides: Synthesis, biological activity, and marketed applications. Eurasian J Sci Technol. 2025; 5(4): 366-384. https://doi.org/10.48309/ejst.2025.512773.1226.
2. Urdiales C, Urdiales-Flores D, Tapia Y, Caceres-Jensen L, Šimůnek J, Antilén M. Transport mechanisms of the anthropogenic contaminant sulfamethoxazole in volcanic ash soils at equilibrium pH evaluated using the HYDRUS-1D model. J Hazard Mater. 2025; 5;487:137077. https://doi.org/10.1016/j.jhazmat.2024.137077.
3. Blasioli S, Martucci A, Paul G, Gigli L, Cossi M, Johnston CT, Marchese L, Braschi I. Removal of sulfamethoxazole sulfonamide antibiotic from water by high silica zeolites: A study of the involved host–guest interactions by a combined structural, spectroscopic, and computational approach. J Colloid Interface Scienc. 2014; 419:148-159. https://doi.org/10.1016/j.jcis.2013.12.039.
4. Fauziyen SP, Saputera WH, Sasongko D. Advancement and prospects in photocatalytic degradation of sulfamethoxazole (SMX) pharmaceutical waste. S Afr J Chem Engineering. 2024; 48(1):375-394. https://doi.org/10.1016/j.sajce.2024.03.008.
5. Elkomy AS, Abdel-Wahab MSh, Shehata N. A comparison between adsorption and photocatalytic degradation for the management of sulfamethoxazole in water. Sci Reports. 2025; 15(1):13576. https://doi.org/10.1038/s41598-025-95947-2.
6. Wajid M, Uzair M, Muhammad G, Siddique F, Bashir M, Nadeem S, Ashraf A, Assad N, Mushtaq A, Rafay MZ, Aqdas A, Ahmad S, Alasmari AF. Sulfamethoxazole-derived Schiff bases: Synthesis, characterization, biological activities, molecular docking, DFT, and ADME studies. J Mol Struct. 2024; 1312(Part 2):138640. https://doi.org/10.1016/j.molstruc.2024.138640.
7. Mushtaq I, Ahmad M, Saleem M, Ahmed A. Pharmaceutical significance of Schiff bases: an overview. Futur J Pharm Sciences. 2024; 10(16):1-12. https://doi.org/10.1186/s43094-024-00594-5.
8. Ghosh SJ, Maity MB, Sepay N, Mahapatra AD, Gupta S, Dutta B, Mahapatra PK, Sinha C. drug action of sulfonamide Schiff bases: Structure, antimicrobial activity and in-silico studies. ESC. Sustainability. 2024; 1:1320. https://dx.doi.org/10.30919/escs1320.
9. Singh C, Adhikari D, Singh BK. Synthesis, spectro-themal characterization, DFT calculations and biochemical evaluation of a newly synthesized tridentate Schiff base transition metal complexes. Polyhedron. 2024; 259:117050. https://doi.org/10.1016/j.poly.2024.117050.
10. Alfonso-Herrera LA, Rosete-Luna S, Hernández-Romero D, Rivera-Villanueva JM, Olivares-Romero JL, Cruz-Navarro JA, Soto-Contreras A, Arenaza-Corona A, Morales-Morales D, Colorado-Peralta R.

Transition metal complexes with tridentate Schiff bases (O N O and O N N) derived from salicylaldehyde: An analysis of their potential anticancer activity. Chem Med Chem. 2022; 17(20): e202200367. https://doi.org/10.1002/cmdc.202200367.

11. Ashok UP, Kollur SP, Anil N, Arun BP, Jadhav SN, Sarsamkar S, Helavi VB, Srinivasan A, Kaulage S, Veerapur R, Al-Rashed S, Syed A, Ortega-Castro J, Frau J, Flores-Holguín N, Glossman-Mitnik D. Preparation, spectroscopic characterization, theoretical investigations, and in vitro anticancer activity of Cd (II), Ni (II), Zn (II), and Cu (II) complexes of 4 (3 H)-quinazolinone-derived Schiff base. Molecules. 2020; 25(24):5973. https://doi.org/10.3390/molecules25245973.
12. Ahmed DS, Emad N, Kadhom M, Yousif E, Al-Mashhadani M. Novel sulfamethoxazole organotin complexes: synthesis, characterization, and hydrogen storage application. Hydrogen. 2024; 5(4): 872-881. https://doi.org/10.3390/hydrogen5040045.
13. Sager AG, Abaies JK, Issa RA. Synthesis, characterization, biological activity, and molecular docking study of some new sulfamethoxazole derivatives. Baghdad Sci J. 2024; 21(11):3411-3427. https://doi.org/10.21123/bsj.2024.9047.
14. Hassanpour H, Naeimi H. Fabrication and characterization of inorganic–organic hybrid copper ferrite anchored on chitosan Schiff base as a reusable green catalyst for the synthesis of indeno [1, 2-b] indolone derivatives. RSC Advances. 2024; 14(24):17296-17305. https://doi.org/10.1039/d3ra08705k.
15. Karaosmanoğlu O, Berber H, Sivas H, Uysal UD. Exploring Schiff bases derived from 2-hydroxybenzaldehyde as potential anticancer agents: Synthesis, characterization, molecular docking and in-vitro evaluation. Cell Biochem Biophys. 2025; 83(4):5051-5069. https://doi.org/10.1007/s12013-025-01826-y.
16. Büyükkıdan N, İlkimen H, Durmuş B, Gülbandılar A. Synthesis and characterization of Cu (II) complexes of proton transfer salts derived from piperazine derivatives and 5-sulfosalicylic acid. Maced J Chem Chem Engineering. 2021; 40(2):159-169. https://doi.org/10.20450/mjcce.2021.2411.
17. Al-Hawarin JI, Abu-Yamin AA, Abu-Saleh AAA, Saraireh IAM, Almatarneh MH, Hasan M, Atrooz OM, Al-Douri Y. Synthesis, characterization, and DFT calculations of a new sulfamethoxazole schiff base and its metal complexes. Materials (Basel). 2023; 16(14):5160. https://doi.org/10.3390/ma16145160.
18. Jarad AJ, Dahi MA, Al-Noor TH, El-ajaily MM, Al-Ayash SR, Abdou A. Synthesis, spectral studies, DFT, biological evaluation, molecular docking and dyeing performance of 1-(4-((2-amino-5-methoxy) diazenyl) phenyl) ethanone complexes with some metallic ions. J Mol Struct. 2023; 1287: 135703. https://doi.org/10.1016/j.molstruc.2023.135703.
19. Khalaf MM, Abd El-Lateef HM, Gouda M, Taha AA, Abdelhamid AA, Abdelbaset M, Alsulami AH, Abdou A. Synthesis, characterization, and in vitro antimicrobial studies of new Mn (II), Fe (III) and Ni (III) complexes based on 4-[(2 sulfanylphenyl) diazenyl] naphthalen-1-ol ligand. J Indian Chem Soc. 2025; 102(2):101601.https://doi.org/10.1016/j.jics.2025.101601.
20. Waheed EJ. Synthesis, characterization and anticancer activity of some metal complexes of new ligand derived from 4-methylbenzohydrazide with computational studies. Iraqi J Pharm Sciences. 2025; 34(2):122-143. https://doi.org/10.31351/vol34iss2pp122-143.
21. Lever ABP. Inorganic Electronic Spectroscopy. 2nd ed. Netherlands, 1984.
22. Arulmozhi S, Sasikumar G, Subramani A, Mohammed MKA, Ali SJA, Ponnusamy S, Jabir MS, Elgorban AM, Zhang W, Natarajan H. Chemical, pharmacological, and theoretical aspects of some transition metal (II) complexes derived from pyrrole azine Schiff base. ACS Omega. 2023; 8(38):34458-34470. https://doi.org/10.1021/acsomega.3c02860.
23. Guney G, Koc ZE. Investigation of dipodal acetoguanamine-Schiff bases and their homonuclear FeIII complexes. J Coord Chem. 2023; 76(13-15):1679-1695. https://doi.org/10.1080/00958972.2023.2262717.
24. Refat MS, Altalhi T, Bakare SB, Al-Hazmi GH, Alam K. New Cr (III), Mn (II), Fe (III), Co (II), Ni (II), Zn (II), Cd (II), and Hg (II) gibberellate complexes: synthesis, structure, and inhibitory activity against COVID-19 protease. Russ J Gen Chem. 2021; 91(5):890-896. https://doi.org/10.1134/s1070363221050194.
25. Singh A, Kumar R, Shiv K, Pandey SK, Bharty MK, Butcher RJ, Prasad LB. Synthesis, crystal structure and screening for anticonvulsant and antianxiety activities of three new Ni (II), Cu (II), and Zn (II) dithiocarbamate complexes. J Mol Struct. 2024; 1298:137052. https://doi.org/10.1016/j.molstruc.2023.137052.

26. El-Habeeb AA, El-Sayed MY, Alatawy IMA, Refat MS. Preparation, spectroscopic and anticancer investigations of metal-drug complexes associated between flumequine antibiotic drug with lanthanum (III), samarium (III) and terbium (III) chloride. Bull Chem Soc Ethiopia. 2024; 38(3):671-684. https://dx.doi.org/10.4314/bcse.v38i3.10.
27. Cary SK, Ferrier MG, Baumbach RE, Silver MA, Pacheco JL, Kozimor SA, La Pierre HS, Stein BW, Arico AA, Gray DL, Albrecht-Schmitt TE. Monomers, dimers, and helices: complexities of cerium and plutonium phenanthrolinecarboxylates. Inorg Chemi. 2016; 55(9):4373-4380. http://dx.doi.org/10.1021/acs.inorgchem.6b00077.
28. Bartosiewicz K, Smortsova Y, Radmoski P, Witkowski ME, Drozdowski KJ, Yoshino M, Horiai T, Szymański D, Dewo W, Zeler J, Socha P, Buryi M, Prokhorov A, John D, Volf J, Runka T, Pędziński T, Hauza K, Jarý V, Shoji Y, Kamada K, Zych E, Drozdowski W, Yoshikawaef A. Shaping scintillation and UV-VIS-NIR luminescence properties through synergistic lattice disordered engineering and exciton-mediated energy transfer in Pr^{3+} doped $Lu_{1.5}Y_{1.5}$ Al_{5-x} Sc_xO_{12} (x= 0.0–2.0) garnets. J Mater Chem. 2025; 13:13691-13712. https://doi.org/10.1039/D5TC01411E.
29. Abbas A, Naqvi SAR, Rasool MH, Noureen A, Mubarik MS, Tareen RB. Phytochemical analysis, antioxidant and antimicrobial screening of Seriphidium oliverianum plant extracts. Dose-response. 2021; 19(1):15593258211004739. https://doi.org/10.1177/15593258211004739.